Automatic monitoring of the bio-colonisation of historical building's facades through convolutional neural networks (CNN)

(Article begins on next page)

AUTOMATIC MONITORING OF THE BIODETERIORATION OF HISTORICAL BUILDING'S FACADES THROUGH CONVOLUTIONAL NEURAL NETWORKS (CNN)

Marco D'Orazio [a*], Andrea Gianangeli[a], Francesco Monni[a], Enrico Quagliarini[a]

[a] Department of Construction, Civil Engineering and Architecture (DICEA), Università Politecnica delle Marche, via Brecce Bianche, 60131 Ancona, Italy

[*] Corresponding author, Tel: +39 0712204587.

Email addressess: m.dorazio@univpm.it (M. D'Orazio), a.gianangeli@univpm.it (A. Gianangeli), f.monni@univpm.it (F. Monni), e.quagliarini@univpm.it (E. Quagliarini)

ABSTRACT

Built cultural heritage is exposed to various deterioration problems caused by different types of actions. To reduce the need for major interventions, preventive conservation (PC) approaches were proposed, based on data collection, regular monitoring, inspections, and control of environmental factors. Monitoring actions able to depict the evolution of buildings' deterioration state, have been proposed and implemented in real cases. Considering that digital images (DI) of historical facades are constantly collected by different subjects and for different purposes, they represent the widest existing data source to support PC approaches and develop predictive tools. DI of historical façades can be used to help in the early recognition of different types of deterioration processes, supporting the creation and application of predictive models based on machine learning (ML) methods. This work proposes a method for the early detection of biological colonization of building facades. A convolutional neural network (CNN) has been trained and tested with images representing the microalgae growth process on historical bricks' facades, collected during experimental activities in controlled conditions. The trained model is characterized by an accuracy of 83% and can recognize the starts of the bio-colonization process on different types of bricks. The trained model has been applied to a historical building used as a case study. The facades of the case study are constantly monitored by surveillance cameras, and DI of the facades are often collected due to the public function of the building. The study shows that by simply processing these images with the trained network it is possible to detect the first stage of bio-deterioration processes. This work is part of a more extensive research for the early detection of different types of building façade damages and can be easily implemented where DI coming from surveillance cameras or other sources are available.

Keywords

Microalgae, biodeterioration, historical buildings, convolutional neural network, monitoring

1 INTRODUCTION

Since the end of the last century, cultural heritage has been increasingly recognized as an important and strategic resource for a sustainable development, and the awareness of its potential for the socio-economic progress of society has constantly grown [1]. Building heritage, due to its material nature, is markedly affected by the factors that contribute to its degradation: physical, chemical, natural and human actions [2].

To preserve this heritage that has come down to us from the past, it is necessary to have intervention strategies tailored for specificities of this field. To this end, it is widely accepted that the PC can be considered the most cost-effective strategy, strongly recommended by international institutions involved in preservation [3]. PC means implementing a strategy of care, based on data collection, regular monitoring, inspections, control of environmental factors and maintenance activities [4]. This concept can be resumed as "a set of actions useful for reducing risk situations concerning cultural assets in their context" [5] [6]. The PC approach starts from a "medical analogy" between the diagnostic process for human and building pathologies [7]. So, following this analogy, damages and defects can be seen as symptoms of a pathology, and therefore a key part of a PC approach is the development of effective "early" damage detection systems, based on the continuous surveillance (i.e., data collection, monitoring activities) of the architectural heritage.

Among the various pathologies that can afflict architectural heritage, attention must certainly be paid to the growth of living microorganisms (bio-colonization). Almost all the historical buildings are affected by primary, secondary or tertiary colonizers such as microalgae (primary), molds, lichens (secondary), plants (tertiary), causing permanent alterations of building facades and relevant costs. The interaction between environmental factors and the physicals and chemicals properties of masonry could be the starting point for a colonization process by primary colonizers, such as microalgae [8][9][10]. The development of these microorganisms has a direct consequence on the material characteristics which are inevitably increasingly degraded with the passage of time and therefore with growth of living organisms that could cause serious losses (especially in the case of cultural heritage buildings) [11]–[16]. Fungi, mould, cyanobacteria, and green microalgae [17] can grow depending on several factors, especially temperature and availability of water, producing chemical and physical degradation of the façade material and becoming a suitable substrate for the growth of other colonizers [18], such as mosses and lichens [8][19][20]. Biological fouling usually starts with the colonization by photoautotrophic microorganisms [8][20] Green microalgae and cyanobacteria (microalgae) are recurrent and they usually develop in combination [9], [21]–[23]. Microalgae can survive at atmospheric temperatures of 5-35/40°C, in rainy, winter and spring seasons. Microalgae require water, but can survive for years to extreme desiccation states and recover full metabolic activity within few hours after rewetting [24]. Roughness and porosity can promote algae growth [25]–[27].

To limit aesthetical, chemical and physical degradation due to bio-colonizers, early detection systems based on data and image collection can be useful.

In the last years many researchers have focused their attention on computer vision-based automated building pathologies identification (using image processing and ML techniques).

An issue that has received a lot of attention is the one of crack detection. Munawar et al. [28] presented a review of image-based crack detection techniques which implement image processing and/or ML. Many works focus on concrete crack detection [29]–[33], not only in the field of existing building but also in the one of infrastructures, like bridges [34]–[39] or roads [40]–[43]. Rezaie et al. [44], Minh Dang et al. [45], Loverdos and Sarhosis [46] focus their works on masonry crack detection.

Several studies oriented on architectural heritage for the automated identification of masonry surface damages by photographing the structure and using ML techniques have also been conducted. Wang et al. [47], [48] used CNN classification techniques to identify and locate several types of damages (like cracks, efflorescence, and spalling) in brick-masonry walls. Remaining in the field of cultural heritage, Wang et al. [49] used CNN for damage identification - such as spalling and area loss - in the roof tiles of a historical building. Zou et al. [50] used CNN to automate the detection of missing components in heritage buildings with particular attention to preventive maintenance activities.

As regard the problem of historical buildings affected by tertiary colonizers (plants) has been addressed the work developed by Ottoni et al. [51] in which is proposed a method for automatic recognition of vegetation on building facades and roofs. Hatir et al. [52] proposed a deep learning method for detection and mapping of stone deterioration in archaeological heritage sites, including the presence of biological colonization.

Regarding the specific identification of microalgae, Chong et al. [53] presents a state-of-the-art of identification methods and ML techniques for image analysis. Pre-processing actions (i.e., resizing, grey-scaling, denoising) and feature extraction methods to apply ML methods (i.e., ANN, CNN, K-NN, DL, SVM) were analysed in depth. The Chong's work shows that CNN (convolutional neural networks) are widely used to identify different types of microalgae species based on DI. However, cited works [54]–[63] are mainly based on images acquired during the growth of microalgae strains in water solution and not on building facades.

The recognition of microalgae on building facades has been analysed in previous works but not in the case of historical facing-masonry walls. In fact, Tran and Hoang [64], [65] proposed a method based on ML techniques for predicting the appearance of algae on building's facades, but in presence of mortar cladding. Valença et al. [66], [67] presented a method designed to detect, analyse and measure areas with biological colonization in exposed concrete surfaces. Considering lack of existing literature, this paper proposes the creation and application of predictive models using CNN able to automatically monitor the biodeterioration status of historical building facades, acting as early detection system.

2 RESEARCH AIM

Following similar approaches where the availability of DI obtained for other purposes is used to detect specific damages [68], and considering that DI of historical facades are constantly collected for different purposes (i.e. surveillance), the aim of present work is to check the ability of a CNN to recognize the growth of microalgae on real images of building facades. Firstly, the CNN was trained using images obtained from an experimental activity and then was applied to a case study to check if the model can recognize microalgae on historical surfaces using common DI (from surveillance cameras or manually collected). The results show as the model trained with laboratory images is able to detect the starts of bio-colonization process with good accuracy. If applied to the case study the method shows a loss of accuracy. It has to be said that the use of common DI could be considered a challenge in several aspects: presence of other elements (e.g., ground, roofs, etc.), low quality, misalignment respect to wall surface plane, significant variation of illuminance. The results can be considered as a starting point towards the creation of tools for early detection of building facades damages using common imagines easy to find.

3 MATERIALS AND METHODS

3.1 Research framework

A four-step research framework has been developed to reach the proposed aim: early identification of bio-deterioration processes on historical building facades. Firstly, an experimental activity (see 3.2) has been organized to follow, in controlled conditions, the microalgae growth process, considering different types of bricks used in the past to realize historical buildings and different types of exposures (temperature, RH%, rain). Then, DI collected during the experimental activity were resized and cropped to obtain a dataset of about 12.000 sub-images (see 3.3), representing the different stages of the bio-deterioration process, and a CNN was trained and tested with the DI dataset obtaining high accuracy (see 3.4). Finally (phase 4), video and DI periodically collected by surveillance cameras during the normal life of an historic building were used to check the ability of the trained network to work in a real case (see 3.5). The whole research framework is depicted in Figure 1.

3.2 Experimental activity

An extended experimental campaign was arranged to obtain the images useful to train the CNN. Five different types of clay bricks (named AH, AL, B, CH and CL) were selected and tested in five different environmental conditions, reproduced using climatic chambers to accelerate the growth process. Bricks differ by color and microstructure (porosity, roughness). Three different brick's colors (light-red, dark-red, yellow) were chosen considering that bio-colonization causes a shift of the original color towards green-blue nuances, and the initial color spectrum is influenced by the shift in wetted and unwetted conditions. Different microstructures were considered because the "shape" of the bio-colonization (i.e., spots. lines, areas) is influenced by the surface characteristics and the water retention ability of the bricks. Finally, different environmental conditions characterized by different temperatures, RH%, and wetting processes were considered to include a wide range of the expected environmental conditions.

To characterize surface properties of the bricks, porosity and roughness were preliminary measured. The total open porosity *P* [%] was determined by a mercury intrusion porosimeter (Micromeritics Autopore III) according to the ASTM D4404-10 standard [69]. The surface roughness R_a [µm] was measured according to UNI EN ISO 4287:2009 standard [70], by using a Taylor Hobson CCI 3D Optical Profiler (Table 1).

To reproduce the bio-colonization process, a green alga (*Chlorella mirabilis* strain ALCP 221B) and a cyanobacterium (*Chroococcidiopsis fissurarum* strain IPPAS B445) were chosen [20], [71], [72]. Microbial strains were cultivated in a Bold's Basal Medium (BBM) prepared in accordance with ASTM D5589-09 standard method [73]. Since a visible biological degradation mostly starts [18] after 1-year or more of natural environmental exposure [74], [75], the use of accelerated tests is recommended. Five different environmental conditions were chosen to consider a wide range of possible real exposures. Three different relative humidity (RH) conditions were reproduced in three separate climatic chambers to investigate their effect on algae growth on fired brick surfaces. The indoor environment was conditioned by saturated solutions, as indicated in EN ISO 12571:2013 [76]. The RH_1 (about 75%) was obtained through a saturated solution of NaCl, RH_2 (about 87%) through a saturated solution of Na_2CO_3, and RH_3 (about 98%) through only deionized water [77]. To only consider the effect of RH, temperature was maintained at 27.5 ± 2.5 °C during all the tests. At the beginning of the test, 9 different points on the surface of each sample were inoculated with 5µL of the mixed culture per point. After the initial inoculation, samples were positioned inside the climatic chambers, inclined at 45° on aluminum-glass racks, front-to-front along the long dimension of the chamber. The test apparatus was placed in a closed room to avoid the influence of light, temperature, and RH of the external environment. Each growth chamber was equipped with two neon lamps (Sylvania TopLife 39W) to provide an adequate illumination equivalent to day/night cycles 14/10 h (Figure 2a).

The influence of temperature on algae growth was carried out following previous researches [25], [26], [72], [78]. Accelerated tests with a periodical water spray on the material surface were performed until the stagnation phase was reached (Figure 2b). Test apparatus consisted of growth chambers (100×40×53 cm^3), filled with 35L of BBM inoculated with the mixed cultures. Algal suspension was sprinkled on sample surfaces (8×8 cm^2) positioned above two aluminum-glass composed racks inclined at 45°. Run/off cycles were set at intervals lasting 15 min and a total of 6 hours per day (3 hours run and 3 hours off). A day/night illumination cycles (14/10 h) were provided by two 39 W neon lamps (Sylvania TopLife).

Considering the available literature [79]–[85], the accelerated tests were set under two different temperatures: 27.5 ± 2.5 °C, that is a temperature within the range of the optimal growth values comprised between 20 °C and 30 °C [79]–[83], and a lower value equal to 10 ± 2.5 °C, within the range of suitable growth [84], [85]. To set the lower test temperature, a modified refrigerator (Electrolux RC 5200 AOW2) was used. Relative humidity was assumed constantly equal to 100% due to the wetting cycles. All the test environments were monitored by temperature and RH sensors (Sensirion SHT31-D), through measurements every 10 minutes.

During each accelerated growth test, analyses were carried out for the evaluation of the algal extent and the biofouling process on samples' surface [25]. Firstly, colorimetric analysis was performed to examine the color variation during time. The chromatic variation (*ΔE*) was measured with a spectrophotometer (Konika Minolta CM-2600dD) [72], [86]. In accordance with UNI EN 15886:2010 and UNI 1602371:2018, results were expressed in CIELAB color space [87], [88]. Color variation was calculated in terms of total color difference ΔE, by equation (1):

$$\Delta E = \sqrt{(L_0^* - L^*)^2 + (a_0^* - a^*)^2 + (b_0^* - b^*)^2} \quad (1)$$

where L^*_0, a_0^*, b_0^* are the color coordinates of samples before the beginning of the test (time zero), and L^*, a^*, b^* the ones measured during the accelerated growth. Measurements were repeated on nine points on each sample surface about every week.

3.3 Image acquisition and splitting

Finally, to train the CNN, DI were weekly collected through a high-resolution scanner (HP Scanjet G3010). The effectiveness of this method has been confirmed in previous studies [9], [25]. The acquired images were elaborated with Imagemagick software as described in the following section. All the images were resized to 1780x1780 pixels using the "imagemagick" tool, rel.7.1.1-20, then cropped to obtain 256x256 sub-images. From each image, 49 sub-images where obtained. All the sub-images were randomly renamed and reordered. Then a manual annotation process was performed. To facilitate the annotation process and considering that microalgae growth causes a color shift towards green values, the image's R, G and B channels were filtered using Matlab software (rel. 2023a). Images showing traces of microalgae were annotated as "algae", and the others as "no_algae". Finally, the annotated dataset of images, consisting of 13.120 sub-images was equally divided into 2 parts, "train" and "test". Each part of the dataset comprises 4780 "algae" images and 1780 "no_algae" images. No filtering actions were performed on resulting images, to check the capability of the trained and tested CNN to work directly with real images [63].

3.4 Convolutional network design, training and testing

A CNN, is a deep learning neural network designed for processing structured arrays of data. CNNs has been successfully applied to various computer vision applications, especially for analyzing visual images and for the multi-category classification (categorizing samples into one of three or more classes) [64]–[68]. A CNN is a feed-forward neural network, comprising many convolutional layers stacked on top of each other, each one capable of recognizing more sophisticated shapes. Pooling layers (subsampling layers) are included. The pooling layer replaces the output of the network at certain locations by deriving a summary statistic of the nearby outputs. This helps in reducing the spatial size of the representation, which decreases the required amount of computation and weights. After a hyper-tuning process, addressed to optimize the number of layers of the CNN a Two-convolution layers CNN was chosen. The first convolutional layer has dimension [32, (3,3)]. The second convolutional layer has the dimension [64, (3,3)] Two pooling layers were included and finally a flatten layer, necessary to convert the resulting matrix into a single array and two dense layers (256,1) have been included. "*Relu*" activation function has been chosen for the convolutional layers and for the first dense layer. "*Sigmoid*" activation function has been chosen for the second "dense" layer. RMSprop optimizer (learning rate = 0.001) has been considered. Considering that we have a binary classification problem, accuracy metric was plotted. Accuracy is the ratio of the number of correct predictions to the total number of predictions made by the model. A batch size of 20 and 50 epochs, for the training process were considered. To train and test the CNN a python script (rel 3.9) has been written. "*Tensorflow*" and "*Keras*" libraries were used to train and test the CNN, "*Keras-tuner*" library has been used to hyper-tune (parameter optimization) the neural network.

3.5 Application to a case study

To show the applicability of the proposed model in real situations, a case study has been chosen. The case study is a 18th century historical building (built from 1733–1743) designed by the Architect Luigi Vanvitelli on an artificial island as a quarantine station for the port town of Ancona called "Mole Vanvitelliana". During the last two centuries, the building has taken different functions: in 1860 as a military citadel, then in 1884 a sugar refinery. Now it is used as a site of a museum, as well as home for various exhibitions. The "Mole Vanvitelliana" main building is rounded by a town-wall. Both the building walls and the town-wall are made with the same type of mortar and bricks. Town-walls are strongly inclined, then the rain can wet the surfaces. It is possible to observe a diffuse biodeterioration process (Figure 3). On the contrary, the facades of the building are vertical and protected by the rain, then not characterized by bio-deterioration.

Two different datasets of images were collected. Firstly, DI extracted from video surveillance HD cameras were collected, to check the applicability of the proposed model to images coming from this type of data source. Then detailed images of the brick facades were manually collected with a HQ resolution camera. All the images were resized [89], [90] to the same dimension (1780x1780) using the "imagemagick" tool, rel.7.1.1-20 and cropped to obtain 773 256x256 sub-images coming from video surveillance cameras and 245 256x256 px images coming from HD cameras. The trained model was iteratively used to check its recognition ability in a real case. Finally, the "accuracy" (number of correct predictions in respect to the number of images) has been computed.

4. RESULTS AND DISCUSSION

4.1 Evolution of the microalgae bio-deterioration process

Figure 4a and Figure 4b shows, respectively, DI and RGB spectrum of the brick's samples (one for each type) before the inoculation (addiction of microalgae spores). Bricks are different by color: B sample is a dark-red brick with the lowest [RGB] spectrum values; AH and AL are light-red bricks with intermediate green [G] spectrum values and high red [R] values; finally, CH and CL are yellow bricks characterized by the highest [RGB] spectrum values.

As can be seen in Figure 5a, microalgae growth initially causes the comparison of little dark green spots (2), then the spots create more large green areas interconnecting with each other (3). These areas assume a typical shape, with largest spots and "filamentous" areas due to the water drainage. In the last phase microalgae growth cause the comparison of light green spots over the initial dark-green spots (4). The shape and the color of these spots and areas can be different depending on the brick's surface characteristics, the growth's phase, and the environmental conditions (Figure 5b).

Figure 6 shows the variation of CIELab mean values (DE) of the brick's surfaces during the experimental activity. Each curve represents the mean values of 27 measurement points (9 points x 3 samples). It is possible to observe a progressive increase of the DE values. DE reached 45-55 values for CH and CL samples after 35 days, 30-35 values for B (after 65 days), and 30-40 values for AH and AL (after 112 days) due to the microalgae coverage. A slight reduction of the peak values has been observed for samples AH and AL after 133 days. Considering that just DE values >= 2 are clearly perceived by the human eye, the color variation is very relevant, reaching a peak of 65 (CL) and confirming the observations made with the DI (Figure 5b).

4.2 CNN training and test

To identify the starts of the microalgae growth process, a CNN has been trained, tested and validated. Figure 7 shows the plot of the history training and test process. At the end of each epoch (iteration on the whole dataset) the accuracy with the "training" dataset and with the "test" dataset has been plotted. The final accuracy (ratio of the number of correct predictions to the total number of predictions made by the model) is 0.83, then 83% of the images with or without microalgae were correctly recognized.

4.3 Automatic identification of microalgae biodeterioration in a case study

To show the applicability of the proposed model, a case study has been selected. The case study is a historical building where security HD cameras are installed, then DI are constantly collected. Moreover, high resolution images are periodically collected during events, due to the public character of the building. DI coming from security cameras nearby the case study were "cropped" to 256x256. The trained CNN was then used to predict microalgae on these images. The application of the trained CNN to this group of images shows that the ability recognition of microalgae on the bricks' surfaces using DI collected through HD security cameras is affected by several factors. Slicing images coming from cameras gives low resolution sub-images, affecting the recognition ability. The accuracy calculated summing the correct predictions over the total number of predictions il low (0.52) if compared to the accuracy calculated on the images of the test dataset (0.83). Moreover, the DI acquired from these cameras includes other elements (ground, roads, roofs, etc.) that were not part of the original dataset. When objects different from the bricks are included in the “cropped” image, CNN frequently fails, reducing total accuracy. Then images with higher resolution are necessary. Moreover, it is necessary to extend the dataset we used to train the CNN also with images including not only the bricks, but also all the elements that it is possible to find on building facades and in the surrounding (Figure 8).

A second group of images directly collected near the building facades and including only bricks with and without microalgae were acquired using an HD camera. Images were resized to 1780x1780 px and cropped to 256x256 px to check the accuracy of the CNN (Figure 9).

In that case, accuracy increases reaching 0.68 value, but remaining lower than the accuracy found at the end of the training ant test procedure (0.83). Then the increase of the resolution combined with the exclusion of elements different than bricks improved recognition ability of the trained CNN. However, the not perfect matching among the colors of the bricks used to train the CNN and the color of the historical bricks in the case study and probably also the presence of other types of bio-colonizers and/or stains reduced the accuracy obtained with real images. It Is important to underline that no filtering actions were performed on images to check the capability of the trained and tested CNN to work directly with real images.

5. CONCLUSIONS

Built cultural heritage is exposed to various deterioration problems that can be caused by different types of actions. To reduce major invasive interventions, a “preventive conservation” approach was proposed, that means a shift from restoration, intended as those activities needed to repair serious deteriorations, to a more inclusive approach, based on a continuous care and supported by data collection, regular monitoring, inspections, control of environmental factors and maintenance activities. Data collection and monitoring actions are a fundamental part of a preventive conservation approach giving the possibility to realize “early” damage detection systems. DI of historical buildings facades (constantly collected by different subjects and for different purposes) represent the biggest available data source to support this approach and can be used to develop predictive tools thanks to the advancements of artificial intelligence methods. This work was addressed to the development of predictive models based on CNN to support a preventive conservation approach. DI of historical façades were used to train a CNN able to recognize bio-colonization phenomena by microalgae on bricks surfaces of historical buildings. The CNN has been trained and tested with images collected during experimental activities. Five different types of bricks were subjected to a bio-colonization process by microalgae and the chromatic alteration of the surface was detected during the growth process. Experimental activities comprised a set of different environmental conditions.

DI collected were cropped to 256x256px to obtain a final dataset of 13.120 images. After a manual annotation process, without filtering actions, two sub-datasets of images (with and without algae) were used to train and test a CNN. The trained model is characterized by an accuracy of 83% and can recognize the starts of the bio-colonization process on different types of bricks. The model has been then applied to a case study to evaluate the ability of the model to recognize microalgae on historical bricks when DI extracted from video surveillance HD cameras and/or HQ DI freely collected are available, as in the case of the case-study. Results shows that the ability for the trained CNN to recognize microalgae on the bricks' surfaces using DI collected through HD security cameras is affected by two main factors. Images extracted from video-surveillance cameras are characterized by medium-low resolution, are captured not orthogonally to the walls and with different illuminance conditions. These aspects affect the recognition ability of the trained CNN, lowering accuracy. On the other side, acquired DI includes other elements (ground, roads, roofs, etc.) that were not part of the original dataset. When objects different from the bricks are included in the "cropped" image, CNN frequently fails. The use of high-resolution images collected on the case study including only bricks facades increases accuracy. An accuracy value of 0.68 was obtained, then lower than the accuracy obtained with the dataset of experimental images. It is important to underline that no-filtering actions were performed on the captured images to check the ability of the CNN to work directly with real images. To overcome the main limit underlined will be necessary to extend this study, increasing the dataset created with experimental activities and including real case images representing all the elements that it is possible to find on building facades and in the surroundings, and images representing different type of bio-colonizers. Despite the declared limitations the proposed model is applicable to real cases to the early detection of microalgae bio-colonization when DI of the details of bricks surfaces are collected.

6. ACKNOWLEDGEMENTS

This research did not receive any specific grant from funding agencies in the public, commercial, or not-for-profit sectors.

REFERENCES

[1] J. Sanetra-Szeliga, *Cultural Heritage Counts for Europe: full report*. 2015. [Online]. Available: http://blogs.encatc.org/culturalheritagecountsforeurope//wp-content/uploads/2015/06/CHCfE_FULL-REPORT_v2.pdf

[2] E. Eken, B. Taşcı, and C. Gustafsson, "An evaluation of decision-making process on maintenance of built cultural heritage: The case of Visby, Sweden," *Cities*, vol. 94, pp. 24–32, 2019, doi: 10.1016/j.cities.2019.05.030.

[3] ICOMOS, "ICOMOS Charter – Principles for the Analysis, Conservation and Structural Restoration of Heritage, Architectural." 2003. [Online]. Available: https://www.icomos.org/en/about-the-centre/179-articles-en-francais/ressources/charters-and-standards/165-icomos-charter-principles-

for-the-analysis-conservation-and-structural-restoration-of-architectural-heritage

[4] K. Van Balen, "Preventive Conservation of Historic Buildings," *Restor. Build. Monum.*, vol. 21, no. 2–3, pp. 99–104, 2015, doi: 10.1515/rbm-2015-0008.

[5] S. Della Torre, "Italian perspective on the planned preventive conservation of architectural heritage," *Front. Archit. Res.*, vol. 10, no. 1, pp. 108–116, 2021, doi: 10.1016/j.foar.2020.07.008.

[6] J. Sroczyńska, "Preventive maintenance of historical buildings in European countries," vol. 2, no. 70, pp. 51–57, 2022, doi: 10.37190/arc220205.

[7] P. B. Lourenço, A. Barontini, D. V. Oliveira, and J. Ortega, "Rethinking preventive conservation: Recent examples," in *Geotechnical Engineering for the Preservation of Monuments and Historic Sites III - Proc. 3rd International Symposium on Geotechnical Engineering for the Preservation of Monuments and Historic Sites – TC301 – IS, Napoli,22-24 June 2022*, London: CRC Press, 2022, pp. 70–86. doi: 10.1201/9781003308867-4.

[8] G. Caneva, M. P. Nugari, O. Salvadori, and ICCROM - International Centre for the Study of the Preservation and the Restoration of Cultural Property, *Biology in the Conservation of Works of Art*. Roma: Sintesi Grafica Srl, 1991.

[9] H. Barberousse, B. Ruot, C. Yéprémian, and G. Boulon, "An assessment of façade coatings against colonisation by aerial algae and cyanobacteria," *Build. Environ.*, vol. 42, no. 7, pp. 2555–2561, Jul. 2007, doi: 10.1016/j.buildenv.2006.07.031.

[10] M. L. Coutinho, A. Z. Miller, and M. F. Macedo, "Biological colonization and biodeterioration of architectural ceramic materials : An overview," *J. Cult. Herit.*, vol. 16, no. 5, pp. 759–777, 2015, doi: 10.1016/j.culher.2015.01.006.

[11] C. C. Gaylarde and P. M. Gaylarde, "A comparative study of the major microbial biomass of biofilms on exteriors of buildings in Europe and Latin America," *Int. Biodeterior. Biodegradation*, vol. 55, pp. 131–139, 2005, doi: 10.1016/j.ibiod.2004.10.001.

[12] C. Gaylarde, M. Ribas Silva, and T. Warscheid, "Microbial impact on building materials: an overview," *Mater. Struct.*, vol. 36, no. 5, pp. 342–352, 2003, doi: 10.1007/bf02480875.

[13] V. P. de F. I. Flores-Colen, J. de Brito, "Stains in facades ' rendering – Diagnosis and maintenance techniques ' classification," vol. 22, pp. 211–221, 2008, doi: 10.1016/j.conbuildmat.2006.08.023.

[14] S. Sannigrahi, F. Pilla, B. Basu, A. S. Basu, and A. Molter, "Examining the association between socio-demographic composition and COVID-19 fatalities in the European region using spatial regression approach," *Sustain. Cities Soc.*, vol. 62, no. July, p. 102418, 2020, doi: 10.1016/j.scs.2020.102418.

[15] G. Caneva, F. Bartoli, M. Fontani, D. Mazzeschi, and P. Visca, "Changes in biodeterioration patterns of mural paintings: Multi-temporal mapping for a preventive conservation strategy in the Crypt of the Original Sin (Matera, Italy)," *J. Cult. Herit.*, vol. 40, pp. 59–68, 2019, doi: 10.1016/j.culher.2019.05.011.

[16] R. Douglas-Jones, J. J. Hughes, S. Jones, and T. Yarrow, "Science, value and material decay in the conservation of historic environments," *J. Cult. Herit.*, vol. 21, pp. 823–833, 2016, doi: 10.1016/j.culher.2016.03.007.

[17] E. Quagliarini, B. Gregorini, and M. D'Orazio, "Modelling microalgae biofouling on porous buildings materials: a novel approach," *Mater. Struct. Constr.*, vol. 55, no. 6, Jul. 2022, doi: 10.1617/s11527-022-01993-x.

[18] O. Guillitte, "Bioreceptivity: a new concept for building ecology studies," *Sci. Total Environ.*, vol. 167, no. 1–3, pp. 215–220, 1995, doi: 10.1016/0048-9697(95)04582-L.

[19] T. Warscheid and J. Braams, "Biodeterioration of stone: A review," *Int. Biodeterior. Biodegrad.*, vol. 46, no. 4, pp. 343–368, 2000, doi: 10.1016/S0964-8305(00)00109-8.

[20] L. Tomaselli, G. Lamenti, M. Bosco, and P. Tiano, "Biodiversity of photosynthetic micro-organisms dwelling on stone monuments," *Int. Biodeterior. Biodegrad.*, vol. 46, no. 3, pp. 251–258, 2000, doi: 10.1016/S0964-8305(00)00078-0.

[21] M. L. Coutinho, A. Z. Miller, and M. F. Macedo, "Biological colonization and biodeterioration of architectural ceramic materials: An overview," *Journal of Cultural Heritage*, vol. 16, no. 5. Elsevier Masson SAS, pp. 759–777, Sep. 01, 2015. doi: 10.1016/j.culher.2015.01.006.

[22] C. Gaylarde, M. Ribas Silva, and T. Warscheid, "Microbial impact on building materials: an overview," *Mater. Struct.*, vol. 36, no. 5, pp. 342–352, 2003, doi: 10.1007/bf02480875.

[23] C. C. Gaylarde and P. M. Gaylarde, "A comparative study of the major microbial biomass of biofilms on exteriors of buildings in Europe and Latin America," *Int. Biodeterior. Biodegrad.*, vol. 55, no. 2, pp. 131–139, 2005, doi: 10.1016/j.ibiod.2004.10.001.

[24] F. C. Carniel *et al.*, "New features of desiccation tolerance in the lichen photobiont Trebouxia gelatinosa are revealed by a transcriptomic approach," *Plant Mol. Biol.*, vol. 91, no. 3, pp. 319–339, 2016, doi: 10.1007/s11103-016-0468-5.

[25] L. Graziani, E. Quagliarini, A. Osimani, L. Aquilanti, F. Clementi, and M. D'Orazio, "The influence of clay brick substratum on the inhibitory efficiency of TiO2 nanocoating against biofouling," *Build. Environ.*, vol. 82, pp. 128–134, 2014, doi: 10.1016/j.buildenv.2014.08.013.

[26] L. Graziani, E. Quagliarini, and M. D'Orazio, "The role of roughness and porosity on the self-cleaning and anti-biofouling efficiency of TiO2-Cu and TiO2-Ag nanocoatings applied on fired bricks," *Constr. Build. Mater.*, vol. 129, 2016, doi: 10.1016/j.conbuildmat.2016.10.111.

[27] T. H. Tran *et al.*, "Influence of the intrinsic characteristics of mortars on biofouling by Klebsormidium flaccidum," *Int. Biodeterior. Biodegradation*, vol. 70, pp. 31–39, 2012, doi: 10.1016/J.IBIOD.2011.10.017.

[28] H. S. Munawar, A. W. A. Hammad, A. Haddad, C. A. P. Soares, and S. T. Waller, "Image-based crack detection methods: A review," *Infrastructures*, vol. 6, no. 8. MDPI AG, Aug. 01, 2021. doi:

10.3390/infrastructures6080115.

[29] J. Valença, E. N. Brito Santos Júlio, and H. J. Araujo, "Intelligent Concrete Health Monitoring (ICHM): An Innovative Method for Monitoring Concrete Structures using Multi Spectral Analysis and Image Processing," in *8th fib PhD Symposium in Kgs. Lyngby, Denmark, June 20-23*, 2010.

[30] B. O. Santos, J. Valença, and E. Júlio, "Detection of cracks on concrete surfaces by hyperspectral image processing," in *Proc, of Automated Visual Inspection and Machine Vision II, 25-29 June, Munich, Germany*, 2017, vol. 10334, pp. 1033407–1/19. doi: 10.1117/12.2269606.

[31] J. Valença, D. Dias-Da-Costa, and E. N. B.S. Júlio, "Characterisation of concrete cracking during laboratorial tests using image processing," *Construction and Building Materials*, vol. 28, no. 1. pp. 607–615, 2012. doi: 10.1016/j.conbuildmat.2011.08.082.

[32] J. Valença, D. Dias-Da-Costa, E. Júlio, H. Araújo, and H. Costa, "Automatic crack monitoring using photogrammetry and image processing," *Meas. J. Int. Meas. Confed.*, vol. 46, no. 1, pp. 433–441, 2013, doi: 10.1016/j.measurement.2012.07.019.

[33] B. Kim and S. Cho, "Automated vision-based detection of cracks on concrete surfaces using a deep learning technique," *Sensors (Switzerland)*, vol. 18, no. 10, Oct. 2018, doi: 10.3390/s18103452.

[34] R. Li, J. Yu, F. Li, R. Yang, Y. Wang, and Z. Peng, "Automatic bridge crack detection using Unmanned aerial vehicle and Faster R-CNN," *Constr. Build. Mater.*, vol. 362, 2023, doi: 10.1016/j.conbuildmat.2022.129659.

[35] H. Wan *et al.*, "A novel transformer model for surface damage detection and cognition of concrete bridges," *Expert Syst. Appl.*, vol. 213, p. 119019, Mar. 2023, doi: 10.1016/j.eswa.2022.119019.

[36] V. Vivekananthan, R. Vignesh, S. Vasanthaseelan, E. Joel, and K. S. Kumar, "Concrete bridge crack detection by image processing technique by using the improved OTSU method," *Mater. Today Proc.*, vol. 74, pp. 1002–1007, Jan. 2023, doi: 10.1016/j.matpr.2022.11.356.

[37] J. Zhang, S. Qian, and C. Tan, "Automated bridge surface crack detection and segmentation using computer vision-based deep learning model," *Eng. Appl. Artif. Intell.*, vol. 115, Oct. 2022, doi: 10.1016/j.engappai.2022.105225.

[38] K. Jang, H. Jung, and Y. K. An, "Automated bridge crack evaluation through deep super resolution network-based hybrid image matching," *Autom. Constr.*, vol. 137, 2022, doi: 10.1016/j.autcon.2022.104229.

[39] J. Valença, I. Puente, E. Júlio, H. González-Jorge, and P. Arias-Sánchez, "Assessment of cracks on concrete bridges using image processing supported by laser scanning survey," *Constr. Build. Mater.*, vol. 146, pp. 668–678, Aug. 2017, doi: 10.1016/j.conbuildmat.2017.04.096.

[40] W. W. Jin *et al.*, "Road Pavement Damage Detection Based on Local Minimum of Grayscale and Feature Fusion," *Appl. Sci.*, vol. 12, no. 24, Dec. 2022, doi: 10.3390/app122413006.

[41] M. Abdellatif, H. Peel, A. G. Cohn, and R. Fuentes, "Pavement crack detection from hyperspectral

images using a novel asphalt crack index," *Remote Sens.*, vol. 12, no. 18, Sep. 2020, doi: 10.3390/RS12183084.

[42] K. Lu, "Advances in deep learning methods for pavement surface crack detection," in *Proc. Conf. Computer Vision and Pattern Recognition, Virtual, 14-19 June*, 2020. doi: https://doi.org/10.48550/arXiv.2012.14704.

[43] L. Zhang, F. Yang, Y. Daniel Zhang, and Y. J. Zhu, "Road crack detection using deep convolutional neural network," *Proc. - Int. Conf. Image Process. ICIP*, pp. 3708–3712, 2016, doi: 10.1109/ICIP.2016.7533052.

[44] A. Rezaie, R. Achanta, M. Godio, and K. Beyer, "Comparison of crack segmentation using digital image correlation measurements and deep learning," *Constr. Build. Mater.*, vol. 261, Nov. 2020, doi: 10.1016/j.conbuildmat.2020.120474.

[45] L. Minh Dang *et al.*, "Deep learning-based masonry crack segmentation and real-life crack length measurement," *Constr. Build. Mater.*, vol. 359, 2022, doi: 10.1016/j.conbuildmat.2022.129438.

[46] D. Loverdos and V. Sarhosis, "Automatic image-based brick segmentation and crack detection of masonry walls using machine learning," *Autom. Constr.*, vol. 140, Aug. 2022, doi: 10.1016/j.autcon.2022.104389.

[47] N. Wang, Q. Zhao, S. Li, X. Zhao, and P. Zhao, "Damage Classification for Masonry Historic Structures Using Convolutional Neural Networks Based on Still Images," *Comput. Civ. Infrastruct. Eng.*, vol. 33, no. 12, pp. 1073–1089, Dec. 2018, doi: 10.1111/mice.12411.

[48] N. Wang, X. Zhao, P. Zhao, Y. Zhang, Z. Zou, and J. Ou, "Automatic damage detection of historic masonry buildings based on mobile deep learning," *Autom. Constr.*, vol. 103, pp. 53–66, Jul. 2019, doi: 10.1016/j.autcon.2019.03.003.

[49] N. Wang, X. Zhao, Z. Zou, P. Zhao, and F. Qi, "Autonomous damage segmentation and measurement of glazed tiles in historic buildings via deep learning," *Comput. Civ. Infrastruct. Eng.*, vol. 35, no. 3, pp. 277–291, Mar. 2020, doi: 10.1111/mice.12488.

[50] Z. Zou, X. Zhao, P. Zhao, F. Qi, and N. Wang, "CNN-based statistics and location estimation of missing components in routine inspection of historic buildings," *J. Cult. Herit.*, vol. 38, pp. 221–230, Jul. 2019, doi: 10.1016/j.culher.2019.02.002.

[51] A. L. C. Ottoni, R. M. De Amorim, M. S. Novo, and D. B. Costa, "Tuning of data augmentation hyperparameters in deep learning to building construction image classification with small datasets," *Int. J. Mach. Learn. Cybern.*, vol. 14, no. 1, pp. 171–186, 2023, doi: 10.1007/s13042-022-01555-1.

[52] E. Hatır, M. Korkanç, A. Schachner, and İ. İnce, "The deep learning method applied to the detection and mapping of stone deterioration in open-air sanctuaries of the Hittite period in Anatolia," *J. Cult. Herit.*, vol. 51, pp. 37–49, Sep. 2021, doi: 10.1016/j.culher.2021.07.004.

[53] J. W. R. Chong *et al.*, "Microalgae identification: Future of image processing and digital algorithm,"

Bioresour. Technol., vol. 369, no. November 2022, p. 128418, 2023, doi: 10.1016/j.biortech.2022.128418.

[54] P. Otálora, J. L. Guzmán, F. G. Acién, M. Berenguel, and A. Reul, "Microalgae classification based on machine learning techniques," *Algal Res.*, vol. 55, no. February, 2021, doi: 10.1016/j.algal.2021.102256.

[55] Z. Zhuo, H. Wang, R. Liao, and H. Ma, "Machine Learning Powered Microalgae Classification by Use of Polarized Light Scattering Data," *Appl. Sci.*, vol. 12, no. 7, 2022, doi: 10.3390/app12073422.

[56] M. E. Sonmez, N. Eczacıoglu, N. E. Gumuş, M. F. Aslan, K. Sabanci, and B. Aşikkutlu, "Convolutional neural network - Support vector machine based approach for classification of cyanobacteria and chlorophyta microalgae groups," *Algal Res.*, vol. 61, no. November 2021, 2022, doi: 10.1016/j.algal.2021.102568.

[57] D. P. Yadav, A. S. Jalal, D. Garlapati, K. Hossain, A. Goyal, and G. Pant, "Deep learning-based ResNeXt model in phycological studies for future," *Algal Res.*, vol. 50, no. May, p. 102018, 2020, doi: 10.1016/j.algal.2020.102018.

[58] G. Pant, D. P. Yadav, and A. Gaur, "ResNeXt convolution neural network topology-based deep learning model for identification and classification of Pediastrum," *Algal Res.*, vol. 48, no. May, p. 101932, 2020, doi: 10.1016/j.algal.2020.101932.

[59] M. Kloster, D. Langenkämper, M. Zurowietz, B. Beszteri, and T. W. Nattkemper, "Deep learning-based diatom taxonomy on virtual slides," *Sci. Rep.*, vol. 10, no. 1, pp. 1–13, 2020, doi: 10.1038/s41598-020-71165-w.

[60] G. Liu, S. Tian, G. Xu, C. Zhang, and M. Cai, "Combination of effective color information and machine learning for rapid prediction of soil water content," *J. Rock Mech. Geotech. Eng.*, Mar. 2023, doi: 10.1016/j.jrmge.2022.12.029.

[61] J. Park, H. Lee, C. Y. Park, S. Hasan, T. Y. Heo, and W. H. Lee, "Algal morphological identification in watersheds for drinking water supply using neural architecture search for convolutional neural network," *Water (Switzerland)*, vol. 11, no. 7, 2019, doi: 10.3390/w11071338.

[62] J. Park, J. Baek, J. Kim, K. You, and K. Kim, "Deep Learning-Based Algal Detection Model Development Considering Field Application," *Water (Switzerland)*, vol. 14, no. 8, pp. 1–14, 2022, doi: 10.3390/w14081275.

[63] S. S. Baek *et al.*, "Identification and enumeration of cyanobacteria species using a deep neural network," *Ecol. Indic.*, vol. 115, no. April, p. 106395, 2020, doi: 10.1016/j.ecolind.2020.106395.

[64] T. H. Tran and N. D. Hoang, "Estimation of algal colonization growth on mortar surface using a hybridization of machine learning and metaheuristic optimization," *Sadhana - Acad. Proc. Eng. Sci.*, vol. 42, no. 6, pp. 929–939, Jun. 2017, doi: 10.1007/s12046-017-0652-6.

[65] T. H. Tran and N. D. Hoang, "Predicting algal appearance on mortar surface with ensembles of

adaptive neuro fuzzy models: a comparative study of ensemble strategies," *Int. J. Mach. Learn. Cybern.*, vol. 10, no. 7, pp. 1687–1704, Jul. 2019, doi: 10.1007/s13042-018-0846-1.

[66] J. Valença, L. M. S. Gonçalves, and E. N. B. S. Júlio, "Assessment of Concrete Surfaces Using Multi-Spectral Image Analysis," in *35th Annual Symposium of IABSE / 52nd Annual Symposium of IASS / 6th International Conference on Space Structures: Taller, Longer, Lighter - Meeting growing demand with limited resources, London, United Kingdom, September*, 2011.

[67] J. Valença, L. M. S. Gonçalves, and E. Júlio, "Damage assessment on concrete surfaces using multi-spectral image analysis," *Constr. Build. Mater.*, vol. 40, pp. 971–981, Mar. 2013, doi: 10.1016/J.CONBUILDMAT.2012.11.061.

[68] S. Bang, S. Park, H. Kim, and H. Kim, "Encoder–decoder network for pixel-level road crack detection in black-box images," *Comput. Civ. Infrastruct. Eng.*, vol. 34, no. 8, pp. 713–727, 2019, doi: 10.1111/mice.12440.

[69] "ASTM D4404-10. Standard test method for determination of pore volume and pore volume distribution of soil and rock by mercury intrusion porosimetry. American Society for Testing and Materials." American Society for Testing and Materials, 2010.

[70] *UNI EN ISO 4287:2009 - Geometrical Product Specifications (GPS) - Surface texture: Profile method - Terms, definitions and surface texture parameters.* International Standards Organization, 2009.

[71] A. Dubosc, G. Escadeillas, and P. J. Blanc, "Characterization of biological stains on external concrete walls and influence of concrete as underlying material," *Cem. Concr. Res.*, vol. 31, no. 11, pp. 1613–1617, 2001, doi: 10.1016/S0008-8846(01)00613-5.

[72] L. Graziani *et al.*, "Evaluation of inhibitory effect of TiO2 nanocoatings against microalgal growth on clay brick façades under weak UV exposure conditions," *Build. Environ.*, vol. 64, pp. 38–45, Jun. 2013, doi: 10.1016/j.buildenv.2013.03.003.

[73] "ASTM D5589-09. Standard test method for determining the resistance of paint films and related coatings to algal defacement. American Society for Testing and Materials." 2009.

[74] H. Barberousse, *Étude de la diversité des algues et des cyanobactéries colonisant les revêtements de façade en France et recherche des facteurs favorisant leur implantation*. 2006.

[75] A. Dubosc, "Etude de devellopement de salissures biologiques sur les parements en beton: mise au point d'essais acceleres de viellissement," *Lab. Matériaux Durabilité des Constr.*, 2000.

[76] "UNI EN ISO 12571:2013. Hygrothermal performance of building materials and products - Determination of hygroscopic sorption properties." 2013.

[77] H. W. Thorp, *Chemical Engineers' Handbook. Second edition (Perry, John H., ed.)*, vol. 19, no. 9. 1942. doi: 10.1021/ed019p449.2.

[78] L. Graziani, E. Quagliarini, and M. D'Orazio, "TiO2-treated different fired brick surfaces for biofouling prevention: Experimental and modelling results," *Ceram. Int.*, vol. 42, no. 3, pp. 4002–4010, Feb.

2016, doi: 10.1016/j.ceramint.2015.11.069.

[79] O. Guillitte and R. Dreesen, “Laboratory chamber studies and petrographical analysis as bioreceptivity assessment tools of building materials,” *Sci. Total Environ.*, vol. 167, no. 1–3, pp. 365–374, 1995, doi: 10.1016/0048-9697(95)04596-S.

[80] G. Escadeillas, A. Bertron, E. Ringot, P. J. Blanc, and A. Dubosc, “Accelerated testing of biological stain growth on external concrete walls. Part 1: Quantification of growths,” *Mater. Struct.*, vol. 42, no. 7, pp. 937–945, 2009, doi: 10.1617/s11527-008-9433-3.

[81] A. Konopka and T. D. Brock, “Effect of Temperature on Blue-Green-Algae (Cyanobacteria) in Lake Mendota,” *Appl. Environ. Microbiol.*, vol. 36, no. 4, pp. 572–576, 1978.

[82] S. P. Singh and P. Singh, “Effect of temperature and light on the growth of algae species: A review,” *Renew. Sustain. Energy Rev.*, vol. 50, pp. 431–444, 2015, doi: 10.1016/j.rser.2015.05.024.

[83] R. Serra-Maia, O. Bernard, A. Gonçalves, S. Bensalem, and F. Lopes, “Influence of temperature on Chlorella vulgaris growth and mortality rates in a photobioreactor,” *Algal Res.*, vol. 18, pp. 352–359, 2016, doi: 10.1016/j.algal.2016.06.016.

[84] J. A. Raven and R. J. Geider, “Temperature and algal growth,” *New Phytol.*, vol. 110, no. 4, pp. 441–461, 1988, doi: 10.1111/j.1469-8137.1988.tb00282.x.

[85] K. Lengsfeld and M. Krus, “Microorganism on façades – reasons , consequences and measures,” no. Venzmer, pp. 0–7, 2001.

[86] J. Radulovic *et al.*, “Biofouling resistance and practical constraints of titanium dioxide nanoparticulate silane/siloxane exterior facade treatments,” *Build. Environ.*, vol. 68, pp. 150–158, 2013, doi: 10.1016/j.buildenv.2013.07.001.

[87] “UNI EN 15886:2010. Conservation of cultural property - Test methods - Colour measurement of surfaces,” 2010.

[88] “UNI 11721:2018. Materiali lapidei - Metodi di prova – Misurazione preventiva della variazione colorimetrica di superfici di pietra.” 2018.

[89] J. W. R. Chong *et al.*, “Microalgae identification: Future of image processing and digital algorithm,” *Bioresource Technology*, vol. 369. Elsevier Ltd, Feb. 01, 2023. doi: 10.1016/j.biortech.2022.128418.

[90] P. Otálora, J. L. Guzmán, F. G. Acién, M. Berenguel, and A. Reul, “Microalgae classification based on machine learning techniques,” *Algal Res.*, vol. 55, May 2021, doi: 10.1016/j.algal.2021.102256.

FIGURE CAPTIONS

Figure 1. Research framework

Figure 2. Test apparatus for the evaluation of relative humidity influence on growth process (a) and for accelerated test aimed at temperature effect investigation (b).

Figure 3. Mole Vanvitelliana, Ancona, Italy.

Figure 4. a) DI of brick's samples before the inoculation of algae spores. From left to right: AH, AL, B, CH, CL. b) [RGB] spectrums of DI of brick's samples before the inoculation of algae spores. From upper to bottom: AH, AL, B, CH, CL.

Figure 5. a) DI of the AL type brick during the microalgae growth process. 1: before microalgae inoculation; 2, 3, 4: after microalgae inoculation. b) Samples of collected DI of the different brick's types during the microalgae growth process.

Figure 6. CIELab variation (DE) of brick's surfaces during microalgae growth process.

Figure 7. Plot of the "training and test" history process. The black line represents the accuracy obtained at the end of each epoch during the training process. The red line represents the accuracy obtained at the end of each epoch during the test process.

Figure 8. Images extracted from HS surveillance cameras and "cropped" to 256x256 px.

Figure 9. Images collected with cameras and "cropped" to 256x256.

TABLES

Table 1. Properties of the bricks used in the experimental activity.

Brick Type	Colour	Total porosity [%]	Roughness [μm]
AR	light-red	19.24 ± 0.37	5.54 ± 0.42
AS	light red	19.24 ± 0.37	4.50 ± 0.27
B	dark red	24.62 ± 1.02	2.95 ± 0.63
CR	yellow	44.09 ± 1.63	7.60 ± 0.57
CS	yellow	44.09 ± 1.63	6.60 ± 0.49

Figure 1


Experimental analysis
35 combinations
5 substrata (AR,AL,B,CR,CL) and 3 sample for each substrata
7 environmental conditions:
T: 5, 10, 27.5, 40 °C
RH%: 75,87,100 %
Digital images collection
Weekly collection of digital images through HQ scanning devices
Image splitting and cropping with imagemagick
13120 images
CNN training, test and validation
2 convolutional layers, 2 pooling layers , 2 dense layers
Batch size = 20, 50 epochs
Accuracy = 0.83
TensorFlow
Keras
Prediction with trained CNN in a case study
On images acquired through:
(1) surveillance cameras,
(2) HD cameras
773 images
245 images
Accuracy = 0.52
Accuracy = 0.68
TensorFlow
Keras
Phase 1
Phase 2
Phase 3
Phase 4

Figure 2

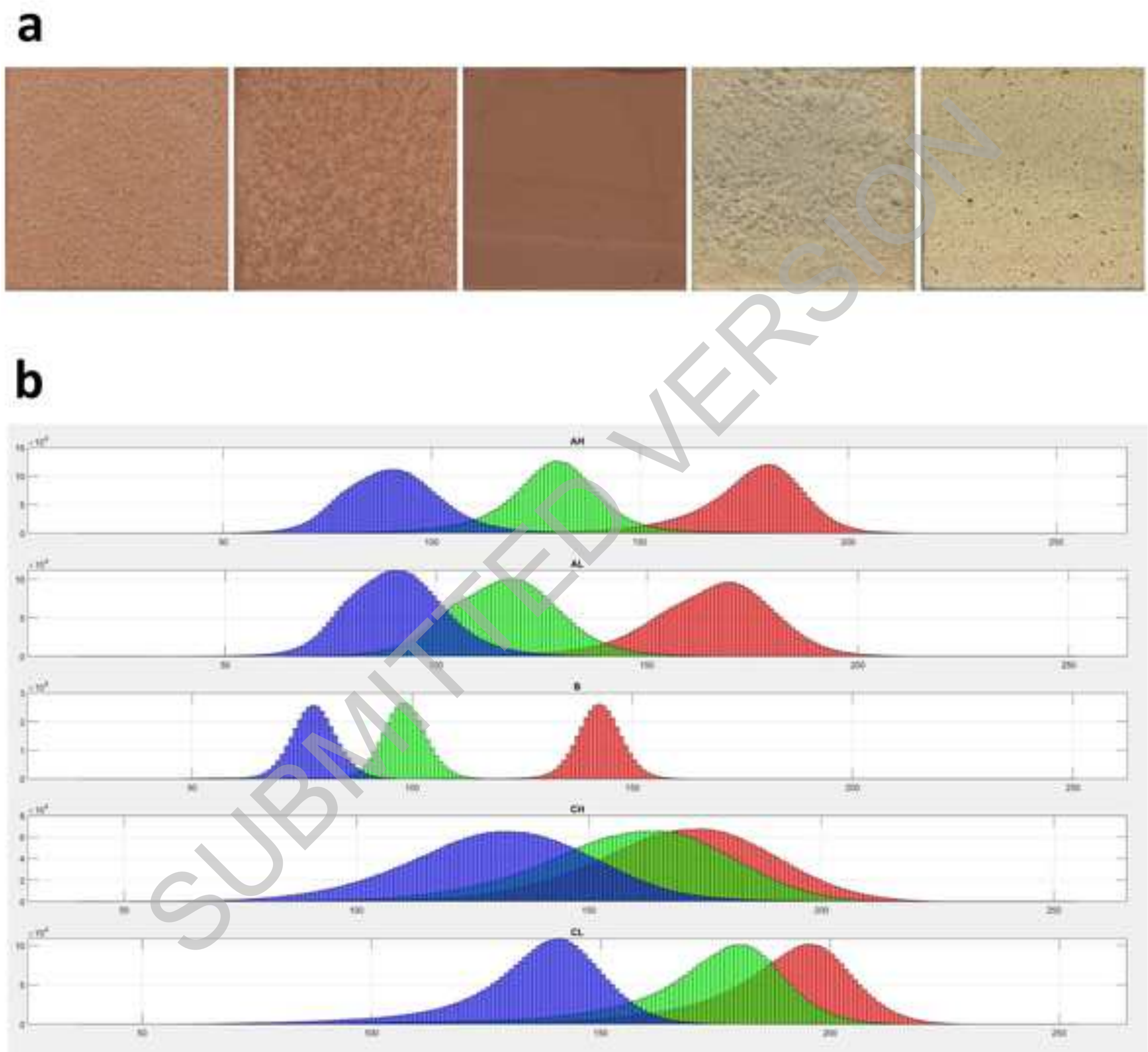
a
b
AH
AL
B
CH
CL

Figure 5

Figure 6

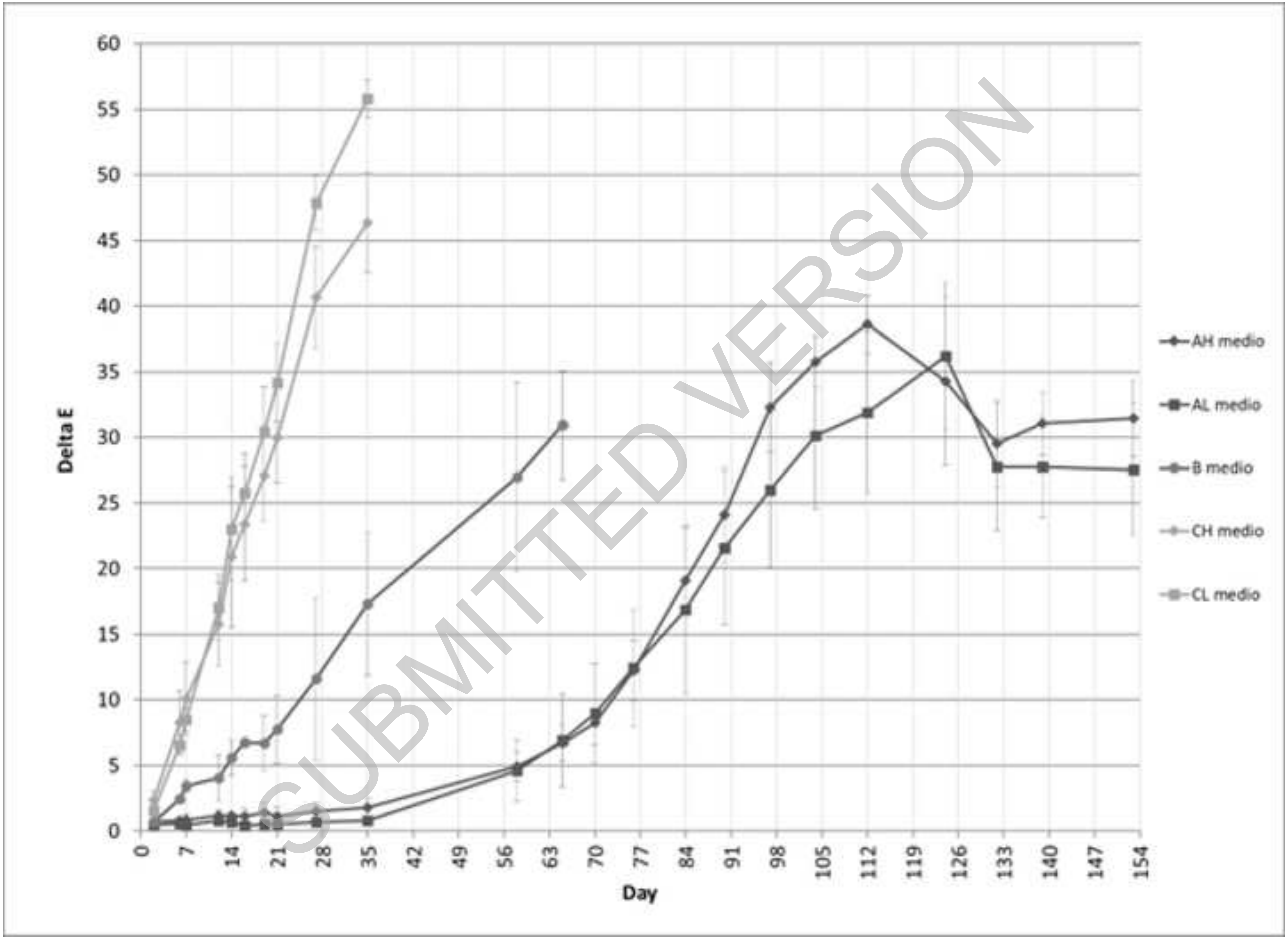
60
55
50
45
40
35
30
25
20
15
10
5
0
Delta E
0
7
14
21
28
35
42
49
56
63
70
77
84
91
98
105
112
119
126
133
140
147
154
Day
AH medio
AL medio
B medio
CH medio
CL medio
SUBMITTED VERSION

Figure 7

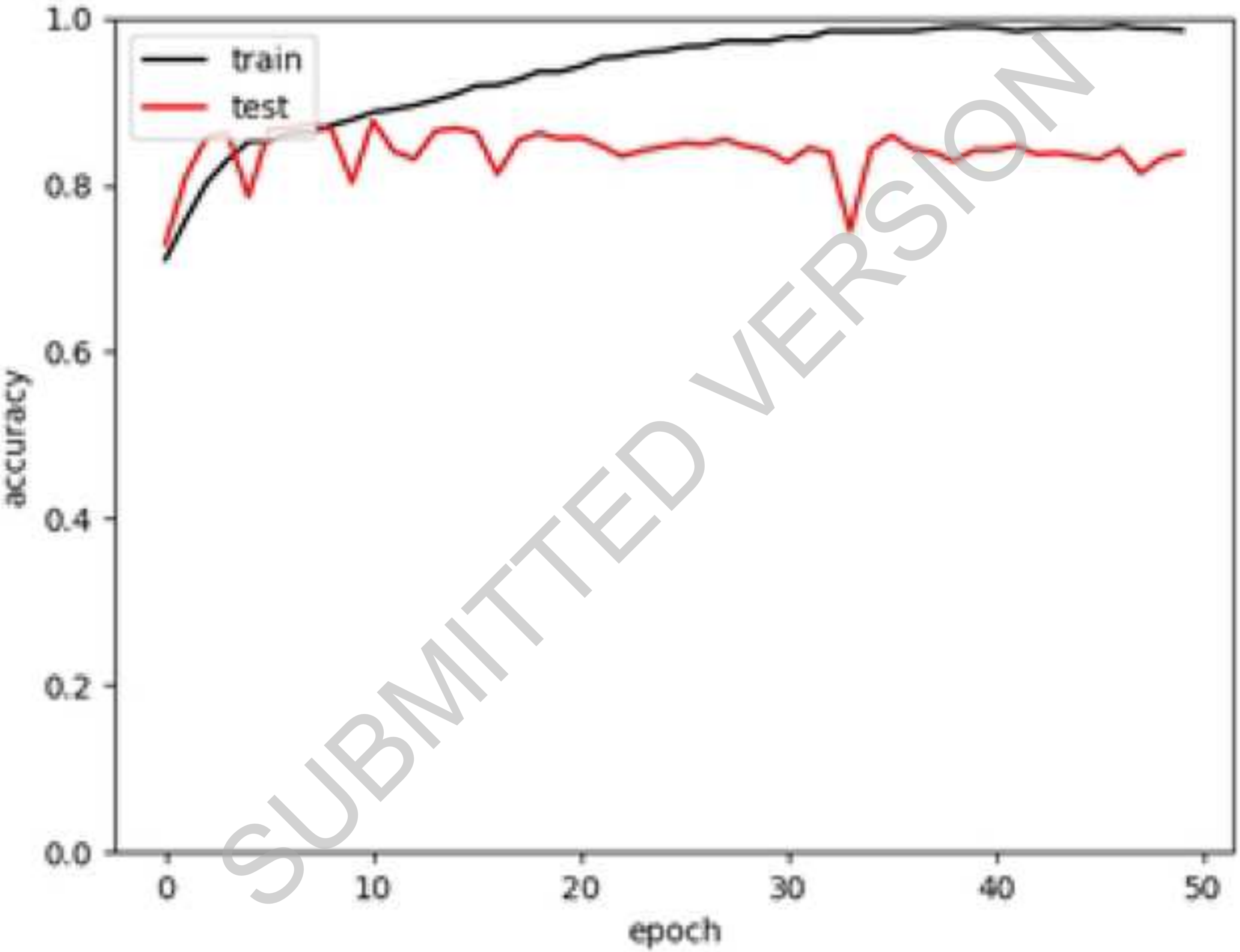

Figure 8

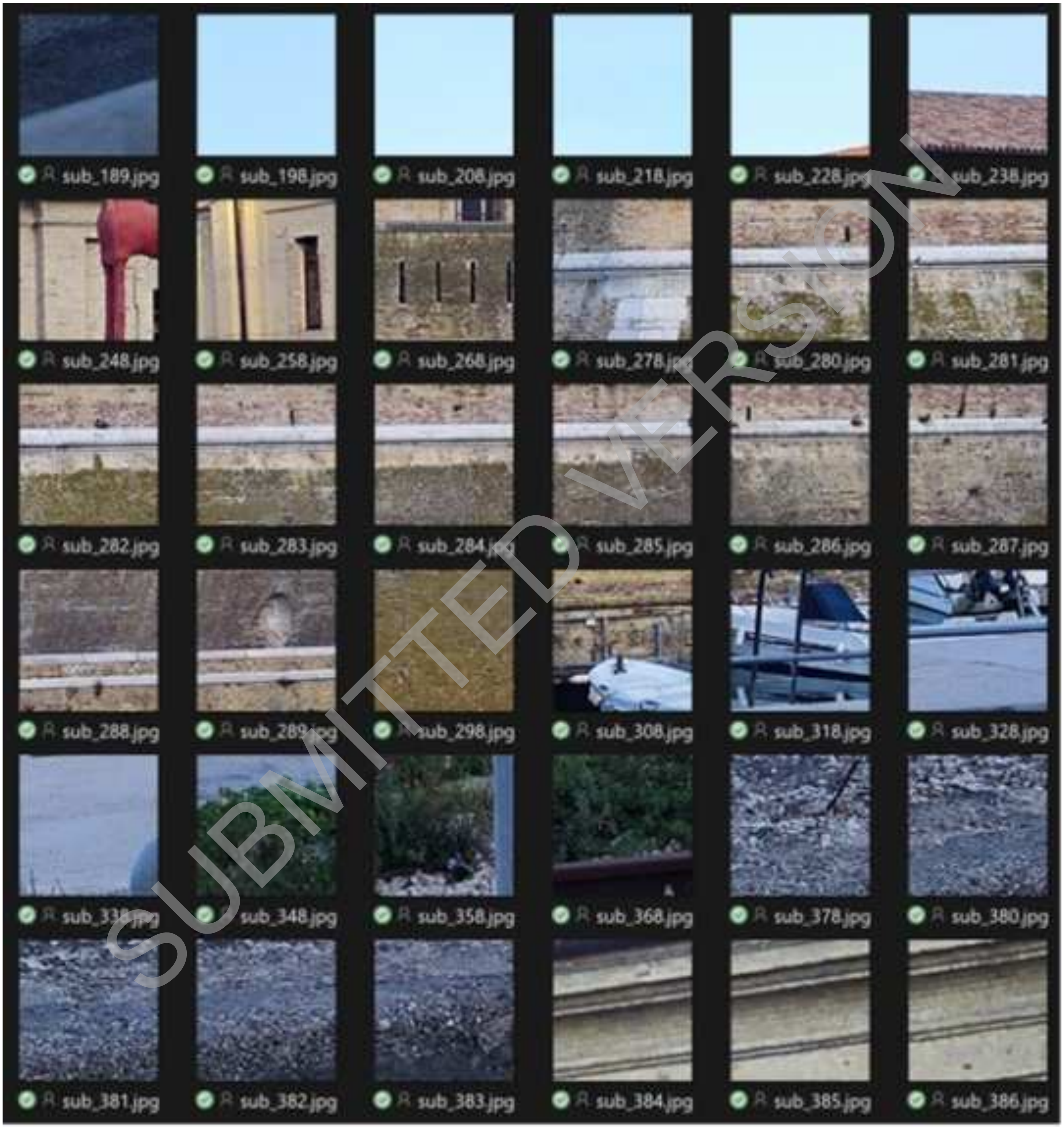
sub_189.jpg
sub_198.jpg
sub_208.jpg
sub_218.jpg
sub_228.jpg
sub_238.jpg
sub_248.jpg
sub_258.jpg
sub_268.jpg
sub_278.jpg
sub_280.jpg
sub_281.jpg
sub_282.jpg
sub_283.jpg
sub_284.jpg
sub_285.jpg
sub_286.jpg
sub_287.jpg
sub_288.jpg
sub_289.jpg
sub_298.jpg
sub_308.jpg
sub_318.jpg
sub_328.jpg
sub_338.jpg
sub_348.jpg
sub_358.jpg
sub_368.jpg
sub_378.jpg
sub_380.jpg
sub_381.jpg
sub_382.jpg
sub_383.jpg
sub_384.jpg
sub_385.jpg
sub_386.jpg

Figure 9

Click here to access/download;Figure(limited to 10);FIG9.JPG.jpg

Brick Type	Colour
AR	light-red
AS	light red
B	dark red
CR	yellow
CS	yellow

Total porosity [%]	Roughness [µm]
19.24 ± 0.37	5.54 ± 0.42
19.24 ± 0.37	4.50 ± 0.27
24.62 ± 1.02	2.95 ± 0.63
44.09 ± 1.63	7.60 ± 0.57
44.09 ± 1.63	6.60 ± 0.49